3D Acquisition of Occluded Surfaces from Scattering in Participating Media

Masaaki Iiyama*, Shohei Miki*, Takuya Funatomi* and Michihiko Minoh*
*Kyoto University
Kyoto, Japan
Email: iiyama@econ.kyoto-u.ac.jp

***Abstract*—Most vision-based 3D acquisition methods including both passive and active methods have a limitation in that cameras must be able to observe the surface to be measured. If this is not possible, that is to say, if the surface is occluded, most of the methods cannot acquire the surface shape. In this paper, we present a method that can acquire the 3D points on the occluded surfaces. The main idea is to observe the scattering of reflected light in a participating medium instead of observing only the reflected light. We place the target in a participating medium, specifically a liquid tank filled with a participating medium, and irradiate a laser beam on it. Even if the reflecting point is occluded, our method can acquire the 3D position of occluded reflecting points from the scattering. Experimental results showed that our method can measure 3D reflecting points on several objects even if the objects are completely occluded.**

I. Introduction

3D shape acquisition of objects is a major task in the field of computer vision, and is of use in various applications, such as modeling for CG production, industrial design, and cultural heritage digitization. Active illumination techniques, including those that involve light stripes and structured light, are widely used to acquire the 3D shape of objects for various applications, and many commercial devices that use these techniques have been developed.

An active illumination technique focuses a light or light stripe onto a target object and estimates the 3D position of the reflected point of the light using a stereo method. Most of these methods are designed under the assumption that the surfaces of targets will reflect light toward cameras so that stereo correspondences can be detected. However, many real-world objects, including mirror-like objects and black matte objects, do not follow this assumption. Although many approaches [1] have been proposed in the literature for measuring such surfaces, none of these approaches can measure occluded surfaces.

This paper proposes an approach for measuring the 3D shape of occluded surfaces. In contrast to previous approaches, we use the scattering of both the incident and reflected light in participating media, instead of only the light reflected toward the cameras.

An overview of our approach is illustrated in Figure 1. We place a target object in a tank filled with participating media (e.g., diluted milk) and focus a laser beam onto the surface of the object. As the laser light passes through the media, some of the light is scattered, and the lights reflected onto the surface are also partially scattered. In this situation, the path of the incident laser beam and the reflected light, which can otherwise not be observed in a clear air environment, can be observed as scattered light. Using the scattered light, we estimate the 2D position of the reflecting point for every image and acquire its 3D position. Because the cameras can observe the scattering of reflected light even when the surfaces are occluded and the light on the surface does not directly reach toward them, our approach is applicable to occluded surfaces that are difficult to be acquired using previous approaches.

II. Related Works

Scattering models are widely used in CG fields, and render various participating media such as fog, smoke. Furthermore, in the field of computer vision, many works have focused on scattering. One such application of scattering is haze removal, in which scattering in the atmosphere is removed from outdoor scene images. He et al. [2] performed haze removal and depth acquisition simultaneously from a single image. Narasimhan et. al. [3] developed a laser range finder and photometric stereo that can be used in the presence of scattering.

Another works related to scattering is the measurement of the scattering effect from images [4]. A work conducted by Narasimhan et al. [5] involved a rich database of the scattering properties of various kinds of objects, and Mukaigawa et al. [6] modeled and analyzed multiple scatterings. While these scattering models help estimate object shapes, few methods actively use scattering for shape acquisition.

A study closely related to ours was performed by Hullin et al. [7]. They used fluorescent material for observing laser trails and succeeded in capturing transparent objects that are difficult to measure using most vision-based methods. In their method, scattering of laser trail is used for shape acquisition. However, this method does not consider a case wherein surface is occluded. Our method considers the scattering of reflected lights in addition to that of the laser trail, and can be applied to the case of occlusion. An acquisition method for scattering objects, i.e., translucent objects, was developed by Inoshita et al. [8]. Their method also actively uses scattering for shape acquisition, but it does not measure occluded surfaces. Furthermore, shape acquisition of underwater objects [9][10] is related to our work. However, none of above these methods can acquire the shapes of occluded surfaces.

In a few works, methods for measuring occluded surfaces were proposed. Sen et al. [11] proposed a method for generating images from the viewpoint of a projector even when no camera is placed at that viewpoint. While this method

1051-4651/14 $31.00 © 2014 IEEE
DOI 10.1109/ICPR.2014.365

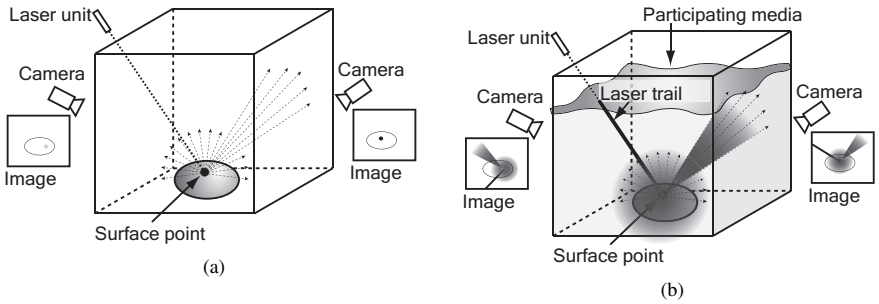

Fig. 1. Overview of our approach. Compared with (a) a traditional active laser range finder, (b) our system observes a laser trail and reflected light as scattering in the participating media.

can be extended for measuring the occluded surface, multiple projectors need to be placed from a non-occluded viewpoint. In contrast, we only require a single laser beam. Most recently, Gupta et al. [12] measured hidden shapes with ultrafast imaging systems. While they used third bounced laser beam for shape acquisition, in this study, we employ the approach of using scattering in participating media. As compared to [12], our method does not need expensive equipments; we use only consumer cameras, a laser beam unit, and a liquid tank.

III. System Configuration

Our system configuration is shown in Figure 1 (b). The system consists of a transparent, e.g., glass or acrylic, liquid tank filled with a participating medium, cameras, and a laser pointer unit. We place the target object inside the tank and irradiate the laser beam on its surface. The cameras are placed such that they can observe the scattering of light in the entire tank. Note that at least two cameras must be used if the laser beam direction is unknown. A single camera is sufficient if the direction can be known using mechanical equipment, e.g., a robot arm or a galvanometer mirror.

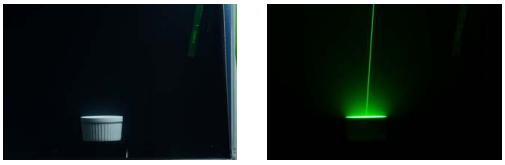

(a) (b)

Fig. 2. Observed image. (a) Image captured in room light environment, (b) image in a darkroom conditions

An example of the input images is shown in Figure 2 (b). Although the reflecting point on which the laser beam is focused is occluded, we can observe that the laser trail and reflection scatter in the participating media. In this study, we solve the problem of detecting the occluded reflecting point in this image without any prior knowledge of its shape.

We model laser beam behavior in the participating media in the following section.

IV. Laser Beam in Scattering Media

A Laser beam radiated from a laser unit travels toward the object's surface. The laser beam is attenuated by the participating media before it reaches the object's surface; in other words, the laser beam is partially absorbed and scattered by the participating media. This absorption and scattering are modeled by Narasimham et. al. [5]. Then, the laser beam is reflected on the object surface and the light reflection are modeled by BRDF. Note that we do not consider subsurface scattering on target objects.

When light travels through the participating media, it hits small particles in the participating media, and the light is partially scattered and absorbed.

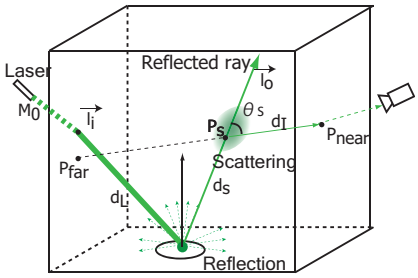

Fig. 3. Scattering in participating media

Let us consider a case in which a laser beam is traveling through the participating media, as shown in Figure 3, and let M_0 be the radiant exitance of the ray. The attenuation inside a participating medium can be modeled as $M = M_0 e^{-\sigma d}$, where d is the traveled distance and σ is the extinction coefficient, which depends on the density and material of the medium. Thus, when the laser beam arrives at the object surface, its irradiance is

$$E_i = M_0 e^{-\sigma d_L}, \tag{1}$$

where d_L is the traveled distance from the wall of the liquid tank to the reflecting point.

The radiance of reflected light in a certain direction, say l_o, is written as, $L_o(l_o) = f(l_i, l_o)E_i$, where l_i and $f(l_i, l_o)$ is the incidence direction and BRDF, respectively. The reflected light is also scattered and absorbed by the participating media. Let P_s be a 3D point on the direction l_o. When the reflected light reaches to P_s, irradiance on P_s can be given by using the distance between P_s and the reflecting point, d_s, as $E(P_s) = \frac{L_o(l_o)}{d_s^2} e^{-\sigma d_s}$, where θ_o is the reflection angle. The radiance of

the scattered light on position P_s is modeled as

$$L_s(P_s, \theta_s) = \beta E(P_s)\mathcal{P}(g, \theta_s), \tag{2}$$

where β is a scattering coefficient and g is a parameter of the Henyey-Greenstein phase function $\mathcal{P}(g, \theta_s)$, which models the angular scattering distribution.

Until $L_s(P_s, \theta_s)$ reaches an image pixel, it continues to be attenuated by the participating medium. Given the traveled distance from P_s to the liquid tank surface, denoted by d_I, the attenuated irradiance can be given by

$$\begin{aligned} L_p(P_s, \theta_s) &= L_s(P_s, \theta_s)\exp(-\sigma d_I) \\ &= \frac{sf(l_i, l_o)\mathcal{P}(g, \theta_s)e^{-\sigma(d_L + d_s + d_I)}}{d_s^2}, \end{aligned} \tag{3}$$

where $s = M_0\beta$.

By integrating equation 3 with the view direction, we can calculate irradiance on an image pixel as

$$I = \int_{P_{near}}^{P_{far}} L_p(P_s, \theta_s) dP_s, \tag{4}$$

where P_{near} and P_{far} are intersections of the view line and the walls of the liquid tank.

Note that this models is only valid under the assumption that no multiple scattering exist. Using a participating media with low scattering coefficient σ, we avoid the effects of multiple scattering.

V. Detection of Occluded Reflecting Points

A. Detection of Object Region and Laser Trail

In the images shown in Figure 2(b), we can observe an incident laser trail as a bright line, the scattering of reflected light as relatively low-intensity pixels outside the object region, and lights multiply reflected on the surface. In this study, we estimate the 3D reflecting point from the laser trail and scattering of reflected light on the surface, and thus, our first step is to extract them from the images. This step consists of (1) masking the object region that may hinder distinguishing the scattering of reflected lights, (2) detecting the laser trail on the image, and (3) reconstructing the 3D laser trail from multiple images.

For masking the object region, we employ a naive background subtraction method that uses pre-captured background and foreground images from a bright scene, as shown in Figure 2(a). We could also have used more sophisticated methods, but masking in our method does not need to be accurate unless the masked region completely covers the entire object region. The remaining process will continue to work correctly even if the masked region contains the scattering region.

In the contrast, the accuracy of the detection of the laser trail strongly affects the overall accuracy of the proposed method. As shown in Figure 2(c), the laser trail is observable in the image, and therefore it can be extracted as follows.

First, the images are binarized, and bright region including the laser trail, namely region A, is extracted, as shown in Figure 4 (b). Second, we apply erosion and dilation operators to remove the line-like shape and acquire a region B. The

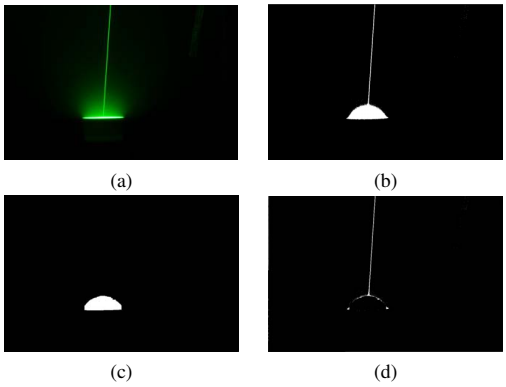

Fig. 4. Detection of object region and laser trail. (a) Input image, (b) region A: binarized image from (a), (c) region B: images after applying erosion and dilation operators, and (d) region C=A-B.

number of iterations of these operators depends on the width of the laser in the image. The laser trail appears as a line-like shape in the image, and the erosion and dilation operators remove the laser trail from region A, as shown in Figure 4 (c). B is subtracted from A, and the line-like region remains. Finally, the Hough transform is applied to this region to obtain the 2D laser trail. Subsequently, the 3D laser trail can be easily acquired from the laser trails captured from different viewpoints. The region of the laser trais is also masked out because it may hinder distinguishing the scattering of reflected light.

B. Estimating the Reflecting Point

The 2D reflecting point in the image is located (a) on an extended line of the laser trail and (b) inside the masked object region. We first select the pixels that satisfy both (a) and (b) as reflecting point candidates. If a candidate p_c is the target 2D reflecting point, the image can be synthesized using equation 4 and p_c that will fit the observed image. One problem is that the BRDF of the target object and the surface normal is unknown, and hence the pixel intensity cannot be calculated. To solve this problem, we focus on intensities of pixels along a line that begins at the 2D reflecting point in a certain direction.

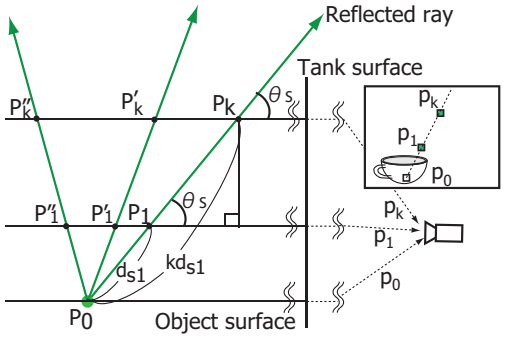

Fig. 5. Viewing rays in the participating media.

Let us consider the following case. There are 3D points P_0, P_1 and P_k along a line, and P_0 is the 3D reflecting point. The

distances between P_0 and P_1, P_0 and P_k are d_{s1} and kd_{s1}, respectively, and these points are projected onto pixels, p_0, p_1, and p_k. For simplicity, we assume that the view lines that pass though p_0, p_1, and p_k are parallel; in other words, the camera projection model is orthogonal or orthogonal-like. Under this assumption, the ratio between the distance from p_0 to p_1 and from p_0 to p_k is $|p_1 - p_0| : |p_k - p_0| = 1 : k$.

When the traveled distance from P_k to the camera, d_{Ik}, compares with that from P_1 to the camera, d_{I1}, it is $(k-1)d_{s1}\cos\theta_s$ shorter than that from P_1, i.e., $d_{Ik} = d_{I1} - (k-1)d_{s1}\cos\theta_s$ From equation 3, the scattering on P_1 and P_k that contribute to the intensities of pixels p_1 and p_k can be written as

$$L_p(P_1) = te^{-\sigma d_{s1}} \tag{5}$$

and

$$L_p(P_k) = t/k^2 \cdot e^{-\sigma(kd_{s1} - (k-1)d_{s1}\cos\theta_s)}, \tag{6}$$

where,

$$t = \frac{sf(l_i, l_o)\mathcal{P}(g, \theta_s)e^{-\sigma(d_L + d_I)}}{d_{s1}^2} \tag{7}$$

The ratio of $L_p(P_k)$ to $L_p(P_1)$,

$$\frac{L_p(P_k)}{L_p(P_1)} = \frac{1}{k^2}e^{-\sigma((k-1)(1-\cos\theta_s)d_{s1})} \tag{8}$$

can be approximated as $\frac{L_p(P_k)}{L_p(P_1)} \approx 1/k^2$ for small values of σ and d_{s1}. These equations can be applicable for other directions, e.g., $\{P_0, P_1', P_k'\}$ and $\{P_0, P_1'', P_k''\}$ in Figure 5.

By integrating equations 5 and 6 with the view direction, the irradiance of pixels p_1 and p_k can be calculated as $I(p_1) = \int L_p(P_1)dP_1 = \int L_p(P_1)d_{s1}d\theta_s$ and $I(p_k) = \int L_p(P_k)dP_k = \int L_p(P_k)kd_{s1}d\theta_s = \int 1/k^2 L_p(P_1)kd_{s1}d\theta_s$, respectively. The ratio of two pixel intensities, p_1 and p_k, can be approximated as

$$\frac{I(p_k)}{I(p_1)} \approx \frac{\int 1/k^2 L_p(P_1)kd_{s1}d\theta_s}{\int L_p(P_1)d_{s1}d\theta_s} = 1/k. \tag{9}$$

Note that the unknown BRDF and surface normal are cancelled out when the ratio is used.

This ratio can be used to calculate the likelihood of a reflecting point candidate. Let p_c be a reflecting point candidate. We draw lines radiating in several directions and extract a set of pixels $\mathcal{L}_\psi(p_c) = \{p_1^\psi, \ldots, p_n^\psi\}$ which are located within the non-object region, as shown in Figure 6. Using p_i^ψ as the pivot pixel, we calculate the pixel intensity of the other pixels of $\mathcal{L}_\psi(p_c)$ as

$$I'(p_j^\psi) = I(p_i^\psi)/k_j, \tag{10}$$

where $I(p_i^\phi)$ is the observed intensity of pixel p_i^ψ and k_j is the ratio of the distance from p_c to p_i and p_c to p_j. Subsequently, the error function can be defined as

$$Err_{\psi,i}(p_c) = \text{med}_j |I(p_j^\psi) - I'(p_j^\psi)|. \tag{11}$$

We use the median as the error function because the observed pixel values may contain *outliers* that occur when the reflected light hits a small particle (e.g., dust in the medium or a scratch on the liquid tank surface).

This error function depends on the pivot pixel and therefore we select a pivot that minimizes $Err_{\psi,i}$. Summing the minimized error over all directions, we define the unlikelihood of a reflecting point candidate as

$$Err(p_c) = \sum_\psi \min_i Err_{\psi,i}(p_c). \tag{12}$$

We calculate this $Err(p_c)$ for all candidates and find the candidate that minimizes $Err(p_c)$ as the 2D reflecting point.

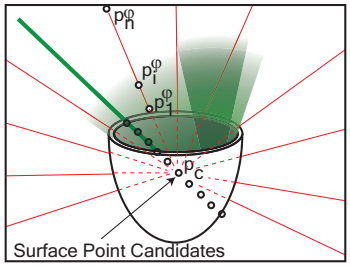

Fig. 6. Reflecting point candidates. The likelihood of p_c is calculated from the pixels on the red lines.

Once the 3D laser beam and the 2D reflecting point are detected, we can easily calculate the 3D reflection point by calculating the intersection between 3D laser trail and the ray which corresponds to the 2D reflecting point p_c. Note that, for 3D laser beam trail has already be known, 2D reflecting points on single image is enough for calculating 3D reflecting point.

VI. Experiments

A. Implementation

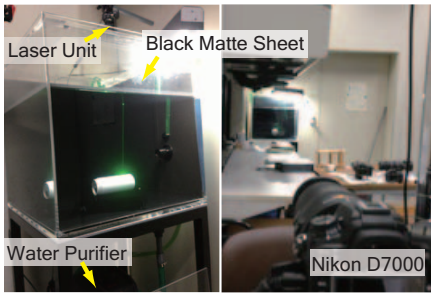

Fig. 7. System implementation. Left: A liquid tank filled with diluted milk and a laser unit. Right: DSLR camera mounted $4m$ away from the walls of the liquid tank

Our measurement system, shown in Figure 7, consists of a 60cm × 60cm × 60cm liquid tank with 9 mm thick crystal clear acrylic walls, two DSLR cameras (Canon D7000 with zoom lenses, 4948 × 3280 pixels) and a 5 mW green laser module (ϕ = 1mm). To avoid reflection of light on the liquid tank surfaces, we covered the background wall of the liquid tank with black matte sheets. We used 1 ml of milk diluted in 180 L water as the participating medium. Referring the discussion and result of Narasimhan's method [5], it is $\sigma = 1.23 \times 10^{-4}(1/mm)$ and $g = 0.714$ in our experiment setup, thus multiple scattering light could be ignored.

Because we assumed an orthogonal projection model, the cameras were placed at a distance of 4 m from the water tank. To reduce the effect of refraction, we placed the cameras orthogonal to the wall of liquid tank.

B. Experimental Results

First, in order to evaluate the accuracy of reflecting point estimation by comparing with ground truth, we used a non-occluded surface as the target objects. We used a white plate whose size was $170mm \times 210mm$, shown in Figure 8(a), as a target object. The plate was placed in the liquid tank as shown in Figure 8(b)-(c), and the laser beam was projected onto 12 points whose positions are indicated by yellow arrows in Figure 8(a). We detected the brightest point on the image and used its position as ground truth of the 2D reflection points.

We masked the images manually, and thus simulated a situation in which the reflecting points were occluded. The white region in Figure 8(d) is a masked (occluded) region. In all our experiments, we used HDR [13] images for detecting reflecting points. Images taken with seven different exposures, from 1s to 30s, were used to create the HDR images.

One of the estimated 2D reflecting points is shown as the red point in Figure 8 (e). The estimation error of this point was 7 pixels, the average error of 12 points was 20 pixels, and errors of eight out of 12 points are within 10 pixels. Considering the radiance of the laser beam is 10 pixels in the image, two third of points are estimated within the spot of the laser beam.

The estimated 3D reflecting points are shown in Figure 8(f). We fit a plane onto the estimated 12 3D points and calculated the error in fitting the plane. Mean error was $1.27mm$, and maximum error was $2.04mm$. These results show that our method can detect reflecting points even when they are occluded.

Second, in order to evaluate whether our method can measure really occluded surfaces, we covered the bottom half of the wall of the liquid tank with black sheets, as shown in Figure 9 (c), and placed target objects at an invisible location from the camera. We used a metal spoon and a white CD-R, as shown in Figure 9 (a)-(b), as target objects. One input images of each of the two objects are shown in Figure 9 (d) and (g). We projected a laser beam onto 70 points on the bowl of the spoon (roughly indicated with a red rectangle) and 31 points on the CD-R, and estimated the 2D and 3D reflection points. Estimated 3D points of both objects are shown in Figure 9 (e),(f),(h), and (i). These results show that the planarity of CD-R and the curvature of the spoon's surface are roughly reconstructed even when the target objects are completely occluded.

Figure 10 (b)-(g) show the observed pixel intensity $I(p_j^{\psi})$ and simulated pixel intensity $I'(p_j^{\psi})$. Figure 10 (b), (c), and (d) correspond to the black, blue, and magenta lines of the left side of Figure 10 (a), respectively, and (e), (d), and (g) correspond to the lines of the right side as in the same manner. While Figure 10 (c) and (f), which correspond to the correct reflecting point, show a strong fit to the observed intensity, Figure 10 (b), (d), (e), and (g), which correspond to ± 30 pixel away from the correct reflecting point, do not fit the observed intensity. This demonstrates that our model properly models the scattering and indicates the location of the reflecting points.

VII. Conclusion

In this study, we developed a new method to measure the 3D position of occluded surfaces. Our method only requires simple devices, such as DSLR cameras, a pointing laser, and a liquid tank, and can estimate the position of occluded points. We utilized the scattering of reflected lights in the participating media to measure the occluded points. Even when the reflected lights were occluded, we could still observe their scattering in most cases, and therefore, it was shown that our method is effective for occluded objects.

A drawback of our method is that it can measure only a single point from one-shot images. Multiple laser beams or structured lights may be used to overcome this drawback, but a more complex observation model than that used in our approach is additionally required. In our future works, we will extend our method to a multiple-laser environment.

References

[1] I. Ihrke, K. N. Kutulakos, H. Lensch, M. Magnor, and W. Heidrich, "State of the art in transparent and specular object reconstruction," *EUROGRAPHICS 2008 STAR–STATE OF THE ART REPORT*, 2008.

[2] K. He, J. Sun, and X. Tang, "Single image haze removal using dark channel prior," *Proceedings on Computer Vision and Pattern Recognition*, pp. 1–8, 2009.

[3] S. G. Narasimhan, S. K. Nayar, B. Sun, and S. J. Koppal, "Structured Light in Scattering Media," in *International Conference on Computer Vision*, Jul. 2005, pp. 420–427.

[4] J. Gu, S. K. Nayar, E. Grinspun, P. N. Belhumeur, and R. Ramamoorthi, "Compressive Structured Light for Recovering Inhomogeneous Participating Media." *PAMI*, pp. –, May 2012.

[5] S. G. Narasimhan, M. Gupta, C. Donner, R. Ramamoorthi, S. Nayar, and H. W. Jensen, "Acquiring scattering properties of participating media by dilution," *ACM Transactions on Graphics*, vol. 25, no. 3, pp. 1003–1012, 2006.

[6] Y. Mukaigawa, Y. Yagi, and R. Raskar, "Analysis of light transport in scattering media," *Computer Vision and Pattern Recognition, 2003. Proceedings. 2003 IEEE Computer Society Conference on*, pp. 153–160, Jun. 2010.

[7] M. B. Hullin, M. Fuchs, I. Ihrke, H.-P. Seidel, and H. P. A. Lensch, "Fluorescent immersion range scanning," in *Acm Transactions on Graphics*, vol. 27, Issue 3, Article 87. Univ British Columbia, Vancouver, BC V5Z 1M9, Canada, 2008.

[8] C. Inoshita, Y. Mukaigawa, Y. Matsushita, and Y. Yagi, "Shape from Single Scattering for Translucent Objects," in *12th European Conference on Computer Vision (ECCV2012)*, 2012.

[9] J. Lavest, G. Rives, and J. Lapreste, "Underwater Camera Calibration," in *Proceedings on European Conference on Computer Vision*, 2000, pp. 654–668.

[10] F. Bruno, G. Bianco, M. Muzzupappa, S. Barone, and A. V. Razionale, "Experimentation of structured light and stereo vision for underwater 3D reconstruction," *International Journal of Photogrammetry and Remote Sensing*, vol. 66, pp. 508–518, Jul. 2011.

[11] P. Sen, B. Chen, G. Garg, S. R. Marschner, M. Horowitz, M. Levoy, and H. P. A. Lensch, "Dual photography," *ACM Trans. Graph.*, vol. 24, no. 3, pp. 745–755, Jul. 2005. [Online]. Available: http://doi.acm.org/10.1145/1073204.1073257

[12] O. O. Gupta, T. T. Willwacher, A. A. Velten, A. A. Veeraraghavan, and R. R. Raskar, "Reconstruction of hidden 3D shapes using diffuse reflections." *Optics Express*, vol. 20, no. 17, pp. 19 096–19 108, Aug. 2012.

[13] P. Debevec and J. Malik, "Recovering high dynamic range radiance maps from photographs," *ACM SIGGRAPH 2008 classes*, pp. 1–10, 2008.

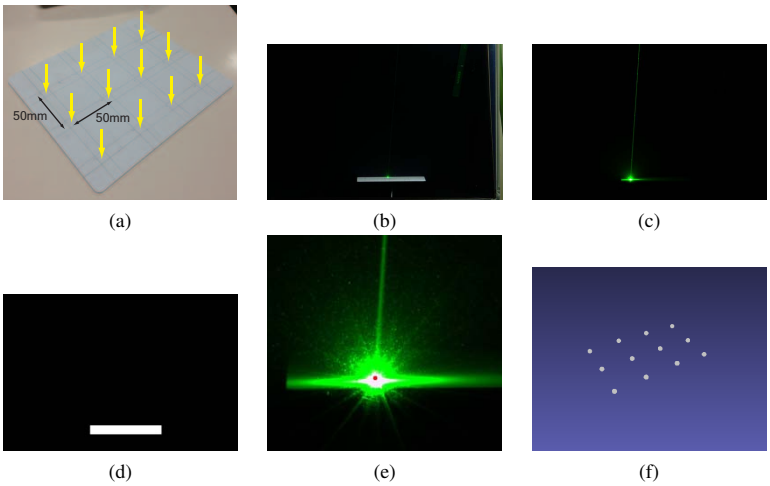

Fig. 8. Experimental results with a white plate. (a) The white plate and 12 reflecting points to be measured, (b) image under indoor lights, (c) image under darkroom conditions, (d) manually masked region indicated by white region. (e) detected 2D points. (f) acquired 3D points.

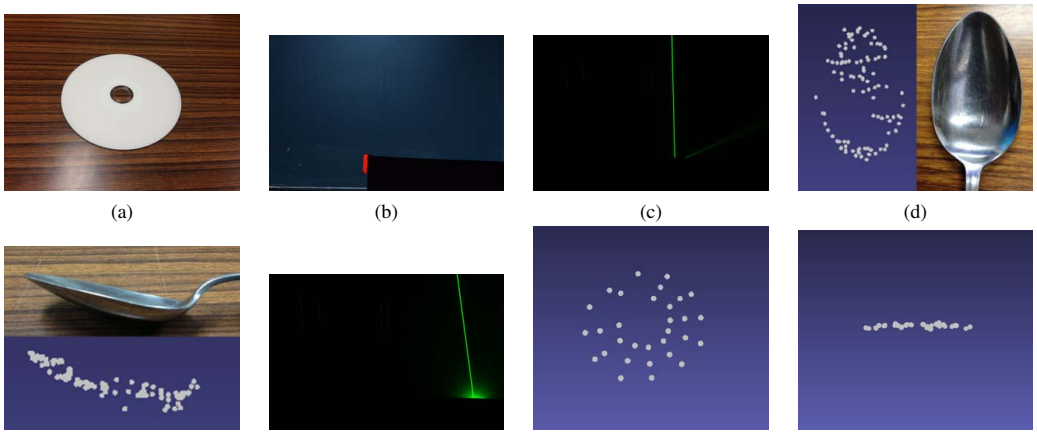

Fig. 9. Experimental results with a metal spoon and CD-R. (a) CD-R to be measured, (b) image in room lighting. Bottom half of the tank wall is covered with sheets. (c) and (f) input images, (d) and (e) reconstructed 3D points of the spoon's bowl. (g) reconstructed 3D points of the CD-R (h) 3D points of the CD-R from horizontal view.

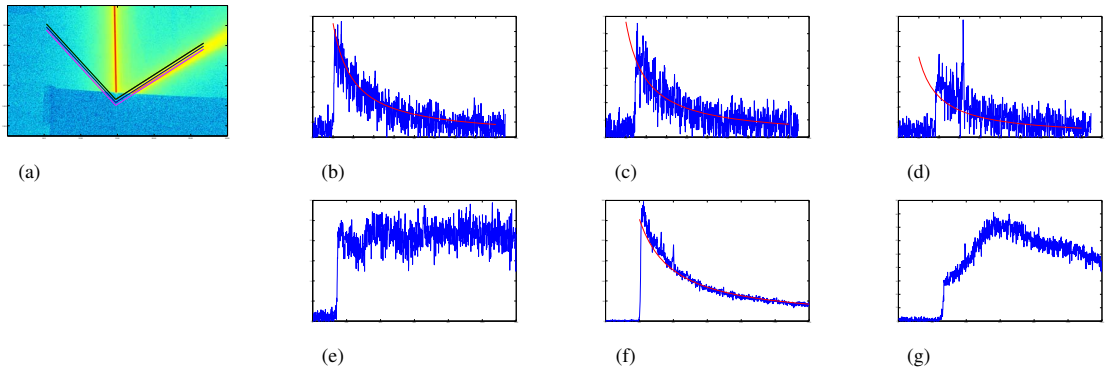

Fig. 10. Observed pixel intensity $I(p_j^{\psi})$. (a) Pixel intensity map. Note that the pixel intensities are displayed as a log scale and converted using a color chart. (b) and (e) correspond to black lines in (a), (c) and (f) correspond to blue lines that pass through the correct reflection point, (d) and (g) correspond to magenta lines. Observed pixel intensity and fitted $1/k$ curve are represented by blue and red lines, respectively.